

Article

Referential Integrity Framework for Lithium Battery Characterization and State of Charge Estimation

Amel Benmouna ^{1,2,*}, Mohamed Becherif ¹, Mohamed Ahmed Ebrahim ³, Mohamed Toufik Benchouia ⁴, Tahir Cetin Akinci ⁵, Miroslav Penchev ⁵, Alfredo Martinez-Morales ⁵ and Arun S. K. Raju ⁵

¹ Institut FEMTO-ST, CNRS, Universite Marie et Louis Pasteur, 90000 Belfort, France; mohamed.becherif@utbm.fr

² School of Business and Engineering, ESTA-UMLP, 90000 Belfort, France

³ Electrical Engineering Department, Faculty of Engineering at Shoubra, Benha University, Cairo 13511, Egypt; mohamed.mohamed@feng.bu.edu.eg

⁴ LGEB Laboratory, Department of Electrical Engineering, University Mohamed Khider, Biskra 07000, Algeria; mt.benchouia@univ-biskra.dz

⁵ Center for Environmental Research and Technology (CE-CERT), Bourns College of Engineering, University of California, Riverside (UCR), Riverside, CA 92507, USA; tahir.cetin.akinci@ucr.edu (T.C.A.); mpenc001@ucr.edu (M.P.); alfredo.martinezmorales@ucr.edu (A.M.-M.); arun@engr.ucr.edu (A.S.K.R.)

* Correspondence: amel.benmouna@utbm.fr

Abstract

The global rise of electric vehicles (EVs) is reshaping the automotive industry, driven by a 25% increase in EV sales in 2024 and mounting regulatory pressure from European countries aiming to phase out thermal and hybrid vehicle production. In this context, the development of advanced battery technologies has become a critical priority. However, progress in electrochemical storage systems remains limited due to persistent technological barriers such as gaps in data, inadequate modeling tools, and difficulties in system integration, such as thermal management and interface instability. Safety concerns like thermal runaway and the lack of long-term performance data also hinder large-scale adoption. This study presents an in-depth analysis of lithium-ion (Li-ion) batteries, with a particular focus on evaluating their charging and discharging behaviors. To facilitate this, a series of automated experiments was conducted using a custom-built test bench equipped with MATLAB (2024b) programming and dSPACE data acquisition cards, enabling precise current and voltage measurements. The acquired data were analyzed to derive mathematical models that capture the operational characteristics of Li-ion batteries. Furthermore, various state-of-charge (SoC) estimation techniques were investigated to enhance battery efficiency and improve range management in EVs. This paper contributes to the advancement of energy storage technologies and supports global ecological goals by proposing safer and more efficient solutions for the electric mobility sector.

Keywords: battery energy storage system; dSPACE data acquisition; electric vehicles; state of charge; state of health



Academic Editor: Yong-Joon Park

Received: 13 May 2025

Revised: 14 July 2025

Accepted: 24 July 2025

Published: 14 August 2025

Citation: Benmouna, A.; Becherif, M.;

Ebrahim, M.A.; Benchouia, M.T.;

Akinci, T.C.; Penchev, M.;

Martinez-Morales, A.; Raju, A.S.K.

Referential Integrity Framework for Lithium Battery Characterization and State of Charge Estimation. *Batteries* **2025**, *11*, 309. <https://doi.org/10.3390/batteries11080309>

Copyright: © 2025 by the authors.

Licensee MDPI, Basel, Switzerland.

This article is an open access article distributed under the terms and conditions of the Creative Commons Attribution (CC BY) license

(<https://creativecommons.org/licenses/by/4.0/>).

1. Introduction

Despite the critical role of Li-ion batteries in enabling the transition to EVs, their development has been hindered by persistent technical challenges. A key issue is the accurate monitoring and control of battery behavior, particularly in estimating the SoC, which is essential for safe and efficient energy management. Inaccurate SoC estimation may lead to performance degradation, reduced battery lifespan, and compromised operational safety.

These challenges highlight the need for advanced modeling and testing methodologies to better understand and manage Li-ion battery systems under varying operating conditions.

SoC estimation techniques are typically classified into three categories: model-based, data-driven, and hybrid methods. Model-based approaches are generally reliable but may suffer from modeling inaccuracies, whereas data-driven methods provide greater flexibility at the cost of requiring large amounts of training data. Hybrid methods seek to integrate the advantages of both strategies [1].

Model-based approaches frequently employ equivalent circuit models (ECMs) or electrochemical models in conjunction with estimation algorithms such as Kalman filters. Among these, Extended Kalman Filters (EKFs) are particularly popular due to their ability to perform recursive state estimation. However, their performance can deteriorate under dynamic conditions, especially when faced with temperature fluctuations and variable load profiles [2]. To address this limitation, an adaptive EKF was introduced that dynamically updates its parameters in real time to account for thermal variations, thereby enhancing SoC estimation accuracy [3]. Building upon this advancement, a temperature-compensated dual EKF was later proposed to concurrently estimate both the SoC and the State of Health (SoH), thus offering a more comprehensive framework for battery diagnostics and management [4].

Hybrid modeling techniques enhance estimation accuracy by combining the electrical properties of ECMs with the physical understanding provided by electrochemical models. These hybrid models have been shown to more effectively capture the coupled thermal and electrochemical behavior of lithium-ion batteries [5]. Their performance is particularly notable under fluctuating load and temperature conditions, where they consistently outperform single-domain models [6]. Additionally, the use of fractional-order Kalman filters—capable of accounting for memory effects and complex internal dynamics—has emerged as a promising direction. These advanced filters have demonstrated substantial gains in estimation accuracy when applied to nonlinear battery behavior scenarios [7,8].

Recent advancements in SoC estimation have increasingly relied on data-driven and machine learning-based techniques. Among these, comparative analyses of neural networks, support vector machines (SVMs), and random forest algorithms have shown that deep neural networks (DNNs) yield the highest prediction accuracy for SoC estimation [9]. Further studies have demonstrated the effectiveness of real-time DNN implementations and neural observers in capturing the nonlinear dynamics of batteries and adapting to varying operational conditions [10–13].

Adaptive estimation frameworks have attracted significant interest due to their capability to handle the dynamic behavior of batteries in EV applications. Methods such as the Adaptive Unscented Kalman Filter (AUKF) and Adaptive Particle Filter (APF) have been shown to enhance robustness against non-Gaussian noise and abrupt load variations, outperforming conventional EKF and UKF techniques [14]. Further refinements have been introduced to improve filter adaptability under battery aging effects, including the use of adaptive forgetting factors that prioritize recent data trends [15].

In parallel, nonlinear observers like Sliding Mode Observers (SMOs) and High-Gain Observers (HGOs) have been explored for their resilience to measurement noise. SMOs, in particular, demonstrate high fault tolerance, although challenges such as chattering and complex tuning remain [16].

With the growing availability of battery data, artificial intelligence (AI)-based techniques have gained traction in SoC estimation. Recurrent Neural Networks (RNNs) and Long Short-Term Memory (LSTM) models are particularly effective at capturing time-dependent characteristics of battery systems, with LSTM models demonstrating superior performance over traditional machine learning algorithms in dynamic driving scenar-

ios [17]. In addition, Convolutional Neural Networks (CNNs), typically applied in image recognition, have been adapted to extract spatial-temporal patterns from voltage and current time series, reducing the need for extensive preprocessing [18].

To mitigate the interpretability challenges of black-box models, Physics-Informed Machine Learning (PIML) has emerged as a compelling hybrid approach. This strategy embeds domain-specific knowledge into machine learning architectures to reduce generalization errors and enhance model transparency [19,20]. Recent work has shown that combining electrochemical models with DNN-based residual correction modules or integrating physical and neural model estimates via Kalman filter-based fusion can deliver both accurate predictions and real-time confidence scores [21].

Modern EV battery management systems are increasingly leveraging multi-sensor data fusion to improve estimation robustness. Ensemble Kalman Filters, for example, have been employed to integrate diverse sensor measurements—such as voltage, current, temperature, and impedance—thus mitigating the impact of sensor drift [22]. Furthermore, combining impedance-based features with time-series data through SVMs has been shown to enhance SoC estimation accuracy, especially under cold-start and high-rate discharge conditions [23].

Quantifying uncertainty in SoC estimation has become increasingly critical to ensure reliability and safety in battery management systems. Techniques such as Bayesian Neural Networks (BNNs) and Monte Carlo Dropout offer the advantage of providing confidence intervals, allowing the model to express its own uncertainty in predictions [24]. Probabilistic graphical models, including Hidden Markov Models (HMMs), have been applied to capture stochastic SoC transitions, particularly under erratic driving conditions [25].

Addressing the effects of battery aging presents an additional challenge. Degradation-aware estimators that treat SoH as a dynamic variable have been developed to compensate for capacity fade and performance loss over time [26]. Hybrid techniques, such as the combination of Recursive Least Squares with Extended Kalman Filters, have enabled joint estimation of SoC and SoH [27], while reinforcement learning approaches trained on long-term degradation data have demonstrated improved adaptability and prediction accuracy in aged batteries [28].

Deploying SoC estimation algorithms in real-time embedded systems introduces computational limitations. Lightweight variants of traditional algorithms—such as optimized EKF implementations for embedded microcontrollers—have achieved high-speed convergence suitable for automotive platforms [29,30]. Memory-efficient Quantized Neural Networks (QNNs) [31] and high-parallelism Field Programmable Gate Array (FPGA)-based implementations [32] have further facilitated the integration of advanced SoC estimation methods in embedded environments.

Considering the diversity in battery chemistries and usage patterns, transfer learning and federated learning have emerged as valuable tools. Transfer learning enables pre-trained SoC models developed for one battery type (e.g., NCA) to be adapted to another chemistry (e.g., LFP) with minimal additional data [33]. Federated learning frameworks allow multiple EVs to collaboratively improve model performance without sharing raw data, thus preserving data privacy [34]. Domain adaptation methods—such as adversarial learning techniques—help translate SoC models trained under controlled laboratory conditions to real-world driving environments [35].

To promote reproducibility and benchmarking, the community increasingly relies on standardized datasets such as NASA's Prognostics Center of Excellence (PCoE), the Oxford Battery Degradation Dataset, and CALCE. Simulation platforms, including MATLAB Simulink BMS Toolbox (2024b), D2CAN, and BATTnet, provide standardized environ-

ments for evaluating SoC estimators under diverse drive cycles like FTP-75 and WLTC. A consolidated comparison of key SoC estimation techniques is presented in Table 1.

Table 1. Comparative analysis for various SoC estimation approaches.

Technique	Strengths	Weaknesses	Key References
EKF/Adaptive EKF	Good accuracy, simple implementation	Sensitive to modeling errors	[6,13]
Dual EKF	Simultaneous SoC and SoH	High computational load	[1,16]
Hybrid Models	High accuracy under load/temp changes	Complex to calibrate	[6,8]
DNN/LSTM	High accuracy, handles nonlinearities	Require large datasets, black box	[12,17]
Fractional Kalman Filter	Captures memory effects, robust	Complex to implement	[7,8]
PIML	Combines accuracy and interpretability	Still experimental	[19]
Bayesian Models	Quantified uncertainty	Slower convergence	[33]

The growing reliance on electric mobility necessitates intelligent battery systems capable of real-time decision-making. Accurate SoC estimation is essential not only for ensuring operational safety but also for enhancing driving range, optimizing charging cycles, and extending battery lifespan. Developing more precise, adaptive, and scalable estimation methods will significantly advance the EV industry while also addressing broader environmental concerns related to transportation emissions.

Recent advancements in SoC estimation and OCV characterization have introduced numerous hybrid approaches combining data-driven and model-based techniques. For example, Kalman filtering methods, adaptive observers, and neural networks are widely used to improve accuracy under varying temperature and current profiles [35–37]. Moreover, physics-informed models that incorporate electrochemical impedance and hysteresis effects have shown promise in enhancing SoC tracking fidelity [38–40]. Integrating such approaches into practical applications remains a challenge, particularly under dynamic operating conditions. Thus, the present work aims to contribute by offering an experimentally validated estimation framework tailored for structured hybrid operating scenarios.

Despite extensive research, a clear gap remains in the practical integration of robust, real-time SoC estimation methods. Existing approaches often struggle to adapt to dynamic load profiles, temperature variations, and battery aging. Furthermore, only a limited number of studies effectively bridge empirical testing and mathematical modeling in a manner that ensures both computational efficiency and estimation accuracy for embedded system applications.

The major contributions of this article can be summarized as follows:

- In-depth experimental analysis of Li-ion batteries was conducted, focusing on their charging and discharging behaviors.
- A measurement bench was designed and implemented, programmed with MATLAB (2024b) and dSPACE DS1104 cards for accurate current and voltage acquisition.
- The acquired data were processed to develop mathematical models that reflect the functional characteristics of Li-ion batteries.

- Suitable SoC estimation techniques were investigated and applied, including model-based and data-driven approaches.
- This study contributes to the development of efficient energy management systems that improve range estimation, battery safety, and overall EV performance.

2. Proposed Test Bench

Accurate characterization of battery behavior under varying operating conditions is fundamental to enhancing the performance and reliability of Battery Management Systems (BMS). In this context, the proposed test bench aims to systematically explore the relationship between the SoC and OCV while also validating charging protocols and sensor calibration. The test environment has been designed with precision instrumentation and controlled parameters to ensure repeatability and practical relevance.

2.1. Experimental Methodology for SoC–OCV Relationship Analysis

The relationship between SoC and OCV is critical for evaluating the performance of rechargeable batteries, especially in applications such as electric vehicles and renewable energy systems. Understanding this correlation allows for accurate estimation of SoC using voltage readings, which is essential for BMS to ensure battery longevity, operational safety, and optimal energy use. To explore this relationship, a comprehensive experimental protocol was implemented under various operating conditions, including different charge/discharge rates and cycling behaviors. The primary objective was to generate a reliable SoC–OCV curve suitable for integration into real-world BMS applications. Data acquisition was performed using a dSPACE DS1104 card operating at a sampling frequency of 10 kHz. Voltage and current signals were synchronized and analogically normalized within the range of [−10 V, 10 V] before entering the board's built-in Analog-to-Digital Converter (ADC). These values were then digitally denormalized within the software to represent actual voltage (V) and current (A) levels. To maintain a manageable data size and reflect the battery's response time realistically, measurements were recorded at one-minute intervals. Analog signal conditioning was achieved using voltage dividers, and preliminary calibration tests were conducted by comparing digitally acquired values with reference readings from a voltmeter and ammeter. This ensured the integrity and reliability of the measured data for further analysis.

2.2. Battery Charge Procedure

This section outlines the experimental steps followed during the battery charging process and includes the corresponding circuit schematic as presented in Figure 1. All tests were conducted at a stable ambient temperature of 25 °C using a new, unused Li-Mn 26650 cylindrical cell. The charging protocol followed the standard Constant Current–Constant Voltage (CC–CV) method, which is widely accepted for lithium-ion batteries due to its balance between efficiency, safety, and cell life. The custom-built test bench integrates dSPACE data acquisition (DAQ) hardware with MATLAB-based control algorithms to enable precise measurement and control of current and voltage during battery cycling tests. The DAQ system is configured with a sampling rate of 1 kHz (1000 samples per second), ensuring sufficient temporal resolution to accurately capture the dynamic response of the lithium-ion battery throughout both charging and discharging cycles. This sampling rate is chosen to support accurate modeling and performance analysis.

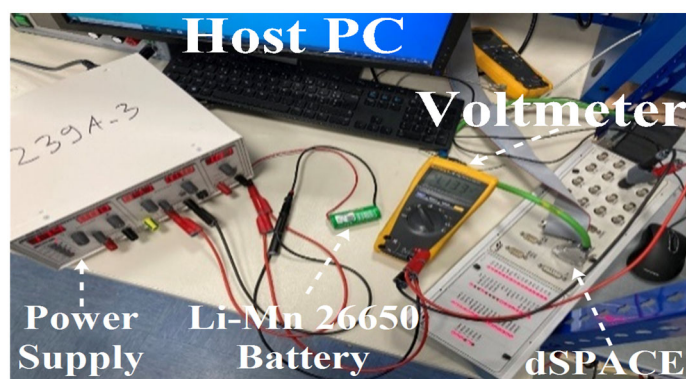


Figure 1. Charging circuit setup.

2.2.1. Constant Current (CC) Stage

In the first stage, the battery was charged at a constant current of 0.9 A, continuing until the terminal voltage reached 4.2 V, which is the upper cutoff limit for the cell.

2.2.2. Constant Voltage (CV) Stage

After reaching 4.2 V, the charger switched to constant voltage mode, maintaining the voltage at that level while the charging current gradually decreased. This phase ended when the current dropped below a set threshold, typically around 0.1 A (C/20 rate), to ensure the cell was fully charged without risking overcharge or lithium plating.

This two-stage CC–CV approach is designed to protect the battery from thermal stress, thereby extending its cycle life and improving overall system safety.

2.3. Battery Discharge Procedure

To evaluate the discharge behavior of the tested Li-Mn 26650 battery, a controlled intermittent discharge protocol was implemented. All experiments were conducted under stable ambient conditions (25 ± 2 °C), with continuous monitoring of both the state of charge (SoC) and open-circuit voltage (OCV) throughout the testing process. The discharge current was regulated using a laboratory-grade programmable DC power supply equipped with multiple output channels, voltage and current adjustment knobs, digital displays, and built-in safety indicators. This setup enabled precise control of discharge conditions while ensuring operational safety. The experimental configuration also incorporated thermal and safety monitoring mechanisms to detect potential anomalies during the cycling procedure. The complete discharge circuit arrangement is illustrated in Figure 2.

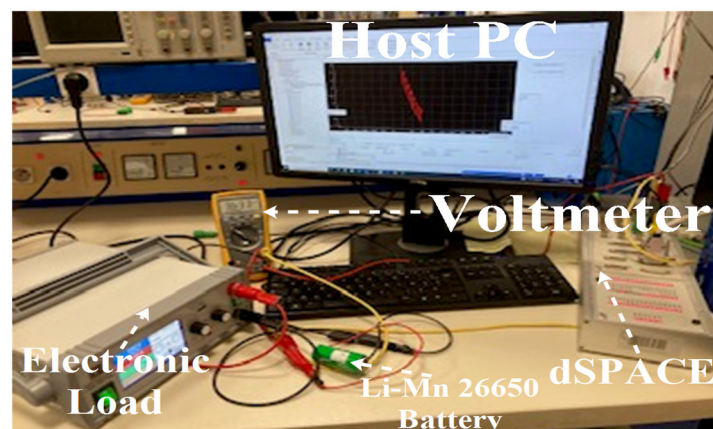


Figure 2. Electrical setup for battery discharge with an electronic load.

The experimental procedure consists of two primary stages:

2.4. Preconditioning Phase

Before initiating the full discharge test, the battery is subjected to a preconditioning phase consisting of 31 controlled cycles to stabilize its electrochemical behavior and simulate intermittent operational conditions. Each cycle involves:

- 10 min of constant-current discharge at 0.8 A;
- Followed by 10 min of rest with no current flow.

This process spans approximately 10.3 h, allowing the battery to be partially cycled in a controlled environment. The rest period was chosen based on preliminary observations indicating that voltage stabilization typically occurs within 4 to 6 min. To ensure consistency and margin, a 10 min rest duration was adopted after each discharge event.

Figure 3 clearly illustrates the evolution of terminal voltage over time during this preconditioning phase. The periodic voltage drops correspond to discharge intervals, while the plateaus represent rest periods where the battery voltage stabilizes. The gradual decrease in voltage over successive cycles reflects the partial energy depletion and dynamic internal adjustments of the battery.

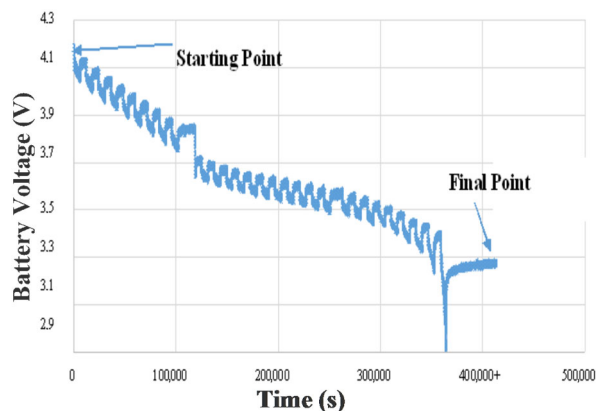


Figure 3. Voltage profile of the battery over time during discharge and rest periods.

It is important to note that aging effects or faulty battery behaviors were not considered within the scope of this study. These aspects are suggested for future research to further explore long-term performance degradation.

Figure 3 depicts the voltage behavior of the battery over the course of 31 preconditioning cycles. A clear pattern of periodic voltage decline during discharge and recovery during rest is observed. This structured fluctuation helps ensure a stable baseline for subsequent discharge tests.

To ensure a well-defined initial SoC, the battery was fully charged prior to the preconditioning phase using a standard constant-current/constant-voltage (CC-CV) protocol. The charging process continued until the terminal voltage reached 4.2 V and the current dropped below 0.05 C, indicating full charge saturation. This procedure established the battery's SoC at 100%. To validate this assumption, the cumulative discharge capacity during the test cycles was closely monitored and found to be consistent with the manufacturer's nominal rated capacity, thereby confirming the reliability of the initial SoC setting.

The selection of 31 preconditioning cycles was based on preliminary experiments and literature guidelines, which suggest that 25–35 cycles are typically sufficient to stabilize battery behavior before conducting precise characterization tests [6,11,13]. During our initial trials, we observed that after approximately 30 cycles, the terminal voltage and SoC variations between successive cycles became minimal, indicating a stable electrochemical state. Therefore, 31 cycles were chosen to ensure consistency while avoiding unnecessary aging, striking a balance between reliability and test efficiency.

2.5. Main Discharge Phase

Following the preconditioning phase, the battery underwent a structured discontinuous discharge protocol lasting approximately 10 h. As depicted in Figure 4, the voltage profile reflects controlled current interruptions and resting intervals designed to assess dynamic performance and relaxation behavior. The discharge was conducted at a constant current of 0.8 A, with periodic pauses allowing the cell to stabilize thermally and electrochemically.

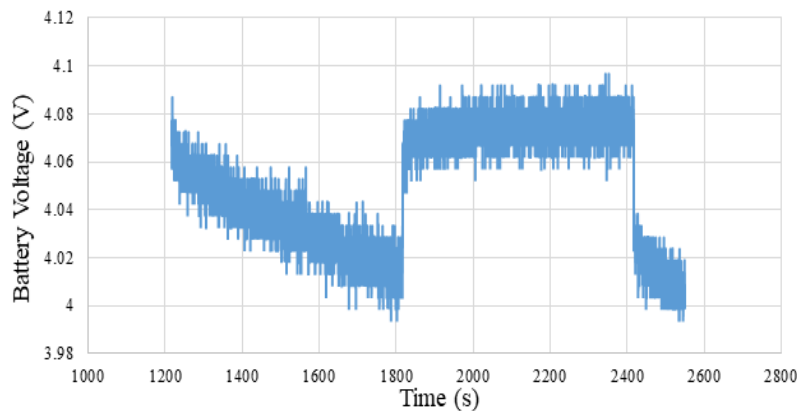


Figure 4. Zoom in of the voltage profile of the battery over time during discharge and one rest period.

To ensure high-fidelity monitoring, key parameters such as terminal voltage, internal temperature, accumulated capacity, and internal resistance were recorded. Data acquisition was performed at one-minute intervals using an integrated Battery Management System, enabling time-resolved analysis of cell behavior under non-steady-state conditions. This detailed voltage trajectory not only validates the consistency of the discharge method but also supports reliable calibration for subsequent state-of-charge estimation and performance benchmarking.

Figure 5 illustrates the complete experimental test bench established to implement the proposed battery characterization and monitoring framework. The setup includes a host PC for control and data acquisition, an electronic load for emulating discharge conditions, a high-precision ammeter for current monitoring, a Li-ion battery under test, and a dSPACE system for real-time hardware-in-the-loop interfacing. This configuration was used to execute discontinuous discharge protocols and rest intervals as part of the preconditioning phase.

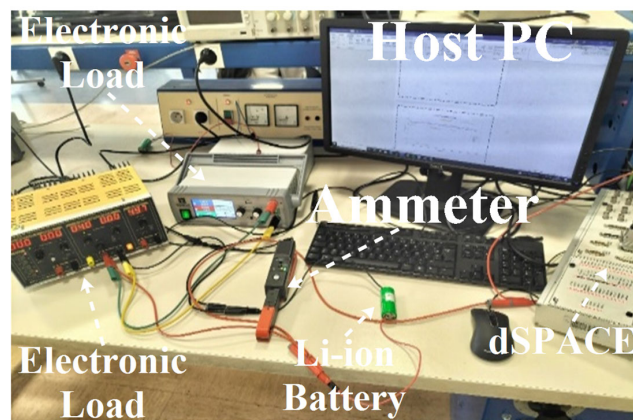


Figure 5. Electrical test configuration for the battery.

Battery current data were acquired using synchronized current sensors, sampled at 1 Hz via a 16-bit analog-to-digital converter. To minimize noise interference and preserve

signal integrity, a second-order low-pass Butterworth filter with a 0.3 Hz cutoff frequency was applied. All sensing channels were time-synchronized to ensure accurate multi-stage correlation during the test cycles. The resulting current profile—monitored and visualized in real-time—was crucial for validating cycle consistency, detecting anomalies, and assessing system reliability across repeated discharge tests.

This experimental platform allowed for continuous feedback, anomaly detection, and referential data tracking in accordance with the Referential Integrity Framework introduced earlier.

Figure 6 illustrates the battery current during the experimental process. Initially, between 0 and 187 s, the battery remains in a rest state with no current flow. At 187 s, a charging current of approximately -1.8 A is applied, which is maintained until 600 s. After this phase, a series of charging and discharging steps is introduced, creating a staircase-like profile that allows for precise SoC and OCV evaluation under varying current loads.

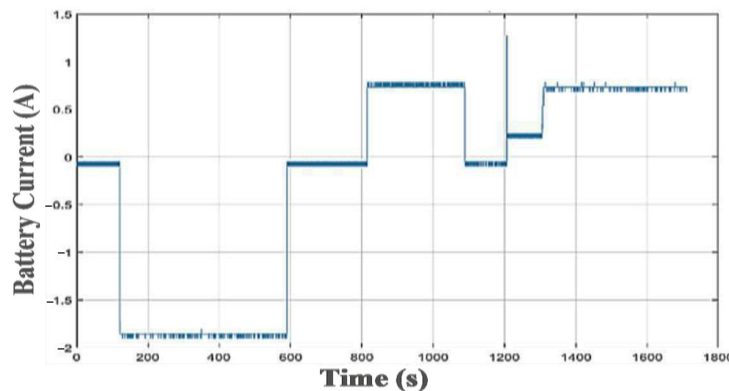


Figure 6. Electrical current curve for the battery.

In Figure 7, the SoC remains stable at around 20% during the initial rest phase. When the charging current is applied, the SoC increases to approximately 29% by 600 s. Following this, the profile reflects both charging and discharging stages, resulting in a gradual decrease in SoC. These dynamic shifts in SoC closely align with the current transitions shown in Figure 6.

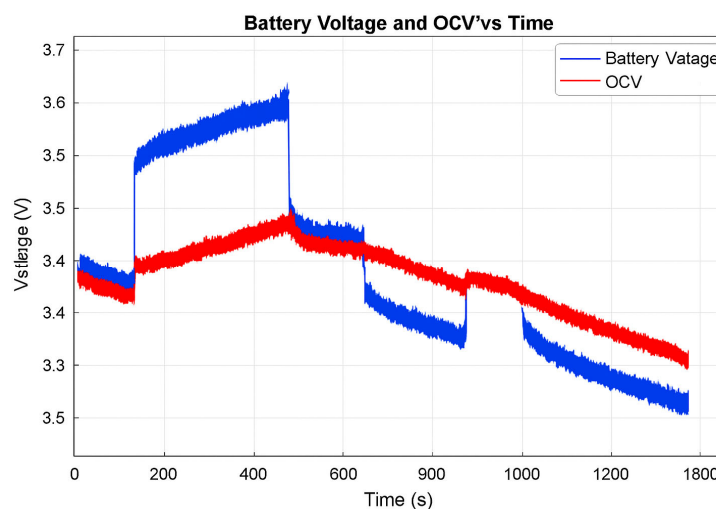


Figure 7. Open circuit voltage and voltage curves for the battery.

Figure 8 presents the measured battery voltage and the corresponding open-circuit voltage (OCV). During rest, both voltages stabilize around 3.46 V. As charging begins, the battery voltage increases more sharply than the OCV, peaking at 3.65 V and 3.53 V,

respectively, around 600 s. The plot clearly highlights the voltage response lag due to internal resistance and electrochemical dynamics.

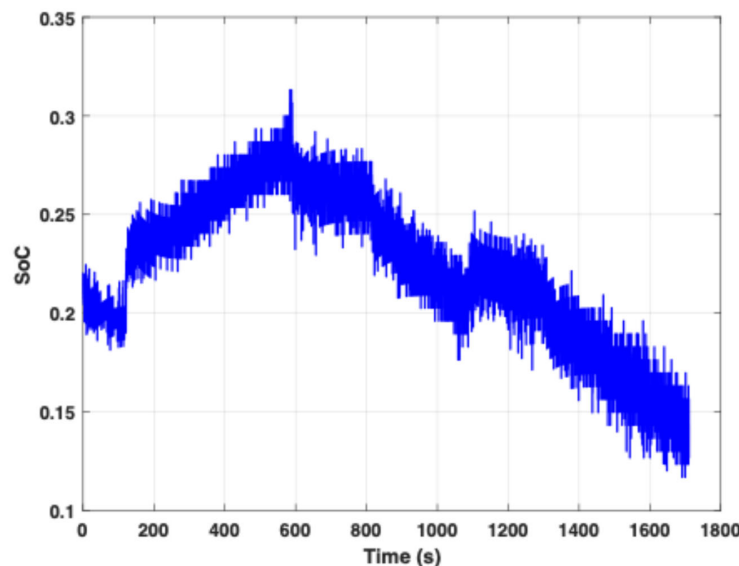


Figure 8. State of charge curve for the battery.

A second idle period occurs between 600 and 800 s, where the current again drops to 0 A. The SoC slightly decreases to 25%, and both the terminal voltage and V_{oc} stabilize around 3.5 V. Between 800 and 1100 s, the battery undergoes a discharge phase under a load of 0.8 A, causing the SoC to fall from 25% back to 20%. The terminal voltage decreases to 3.42 V, and the V_{oc} holds at 3.46 V. During this period, hybrid operation is initiated: a total load of 1.8 A is applied, but the DC source supplies only 1 A, requiring the battery to provide the remaining 0.8 A. This leads to further SoC depletion from 22% to 13%, confirming the battery's active role in load sharing. Another short resting interval follows between 1100 and 1200 s, during which the SoC recovers slightly to 22%, and the voltages stabilize at 3.49 V (V_{bat}) and 3.46 V (V_{oc}). In the final phase, from 1200 to 1700 s, hybrid mode resumes with the same 1.8 A load. The battery again compensates for the current shortfall, reducing the SoC to 13%, the battery voltage to 3.37 V, and the V_{oc} to 3.44 V. Throughout the experiment, V_{oc} serves as a reference voltage. During hybrid operation, the battery acts as a current source in parallel with the load, as evidenced by the drop in voltage (from 3.49 V to 3.37 V) and corresponding SoC decrease. Coulomb counting-based method for SoC estimation: This approach uses current as an input and calculates SoC by integrating current over time. A key limitation of this method is that it requires a known initial SoC, which may be estimated using methods such as Electrochemical Impedance Spectroscopy (EIS) or Extended Kalman Filter (EKF). In our lab experiments, the initial SoC is known, and the final SoC values obtained from the Coulomb counter are stored and used as the starting point for subsequent tests. The Coulomb counter is defined by Equation (1).

Among various SoC estimation techniques, Coulomb Counting remains one of the most widely implemented due to its simplicity and suitability for real-time embedded applications. Unlike more complex approaches such as Kalman Filtering, Model-Based Estimation, or Machine Learning-driven methods, Coulomb Counting does not require intensive computation or a detailed electrochemical model of the battery. This makes it particularly advantageous in resource-constrained systems where real-time performance is prioritized.

However, this simplicity comes with limitations. Coulomb Counting is sensitive to cumulative sensor drift, current measurement errors, and inaccurate initial SoC settings.

Despite these drawbacks, it remains a practical choice when used in tightly controlled environments with periodic recalibration, as in the present study. Its straightforward implementation enables consistent and interpretable measurements, supporting the study's focus on validating a referential integrity framework for battery testing.

The Coulomb Counting method is a widely adopted technique for estimating the SoC by integrating the measured charge and discharge currents over time. Although it offers a straightforward implementation, especially in embedded systems, the accuracy of this method can degrade over prolonged use due to accumulated errors from sensor drift, current integration noise, or initial SoC estimation inaccuracies. These limitations necessitate regular recalibration or hybrid estimation methods, particularly in applications requiring high reliability, such as electric vehicles or aerospace systems. In this study, Coulomb Counting is applied under tightly controlled laboratory conditions, minimizing environmental and sensor-related deviations to ensure high-quality data acquisition.

In this study, all experiments were conducted in a climate-controlled laboratory environment, where ambient temperature was maintained at 25 ± 1 °C and humidity levels were kept below 45%. The battery under test was isolated from external airflow and radiant heat sources, and all current and voltage measurements were captured using calibrated high-precision equipment (Keysight 34461A multimeter and BK Precision 8500B DC load). To minimize electromagnetic interference and ensure stable signal acquisition, shielded cabling and a dedicated measurement chamber were used. These controlled conditions ensured consistent data acquisition, minimized thermal drift, and improved the reproducibility of results.

$$\text{SOC} = \text{SOC}_0 - \frac{1}{C_N} \int_{t_0}^t i_{batt} d\tau \quad (1)$$

where C_N is the rated capacity, i_{batt} the battery current, and SOC_0 is the initial SOC.

Despite its simplicity, this method has several drawbacks, including the sensitivity to the initial SOC value that could be inaccurately estimated and the accumulated error due to the use of integration. The estimation accuracy is influenced by the temperature and other internal battery effects, such as self-discharge, capacity loss, and discharging efficiency. However, this method is largely used even by car manufacturers.

3. Investigation of Battery State of Charge Estimation During Discharge and Rest Cycles: Methodology and Results

3.1. Experimental Methodology for SoC–OCV Relationship Analysis

As part of this study, an experimental procedure was developed to examine the relationship between OCV and SoC in a battery. The protocol consisted of 30 sequential discharge–rest cycles, enabling systematic data collection for reliable analysis.

Each cycle involved a controlled discharge at a constant current of 0.8 A, followed by a rest period to allow the battery voltage to stabilize. This method ensured accurate measurement of OCV at varying SoC levels.

The key parameters selected for battery behavior modeling include:

- (i) Nominal battery capacity (q_1);
- (ii) Discharge current of 0.8 A;
- (iii) Total of 30 discharge cycles.

The maximum battery capacity (Q_{\max}) is calculated as 4.133 Ah using the expression:

$$Q_{\max} = \frac{0.8 \times 600 \times 31}{3600} \quad (2)$$

This formula accounts for discharge current, cycle duration in seconds (600 s per cycle), total cycles, and conversion from seconds to hours.

The SoC at a given cycle number (n) is computed using the formula

$$SoC(n) = \frac{q_1 \times n}{Q_{max}} \quad (3)$$

This equation tracks SoC evolution by integrating the nominal capacity and the number of completed cycles. The methodology provided a reliable framework for mapping OCV to SoC, offering valuable insights for battery management and optimization strategies. Moreover, in the performed experiments, each discharge–rest cycle is followed by a two-hour rest interval. This duration is selected based on preliminary testing, which indicated that a two-hour rest is typically sufficient for the battery voltage to approach its equilibrium, or open-circuit voltage (OCV), particularly for the specific cell type and capacity used in this study. To ensure accurate OCV measurements, the authors applied a stabilization threshold and continuously monitored the voltage during the rest period. The rest interval is considered complete only when the voltage change is less than 5 mV per minute for a continuous 10 min duration. The authors acknowledge that battery aging and efficiency losses over multiple cycles can influence capacity and voltage behavior. While aging effects are not explicitly modeled in this study, the authors monitored capacity fade and internal resistance throughout the 30-cycle testing protocol. The results showed minimal degradation, with capacity loss remaining below 1%.

3.2. Experimental Setup and Data Acquisition

To ensure data consistency, traceability, and comparability throughout the battery testing process, a structured experimental workflow was developed based on the Referential Integrity Framework (RIF). This framework integrates all acquisition steps and safety control operations into a coherent and repeatable structure. As illustrated in Figure 9, the process begins with a clearly defined test cycle, followed by tightly controlled charging and preconditioning phases.

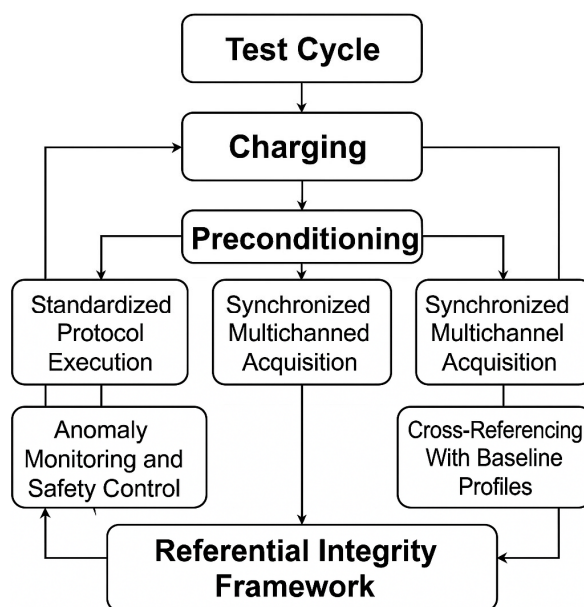


Figure 9. Workflow of the referential integrity framework, including synchronized multichannel acquisition, anomaly detection, and standardized protocol execution steps under controlled charging and preconditioning cycles.

During these stages, standardized protocol execution and synchronized multichannel acquisition occur concurrently, ensuring time-aligned, high-resolution data collection across multiple channels and sensors. To safeguard against potential anomalies, the system incorporates real-time anomaly monitoring and safety control mechanisms, thereby minimizing the risk of test failure or data loss.

The cross-referencing with baseline profiles step serves to validate new measurements against reference data, reinforcing the integrity and reliability of the collected dataset. All outputs ultimately feed into the Referential Integrity Framework, which functions as an overarching supervisory layer to maintain data authenticity and reproducibility. This visual flow not only elucidates the internal logic of the testing methodology but also strengthens the transparency and repeatability of the entire study.

4. Experimental Results and Discussion

This section presents a comprehensive evaluation of how varying initial SoC and applied current levels influence the charging and discharging characteristics of lithium-ion batteries. The findings are supported by experimental data to ensure real-world applicability and technical clarity.

Influence of Initial State of Charge and Current Levels on Charging and Discharging Durations

Understanding the relationship between SoC, current levels, and time efficiency is critical for optimizing battery operation. This subsection highlights the practical implications of the current magnitude and starting voltage on both charging and discharging profiles.

To visualize and support the effects discussed above, Figures 10–15 illustrate the battery voltage profiles under varying current levels and initial SoC values during both charging and discharging phases. Each figure is discussed in detail below to highlight the impact of the current magnitude on process duration and voltage behavior.

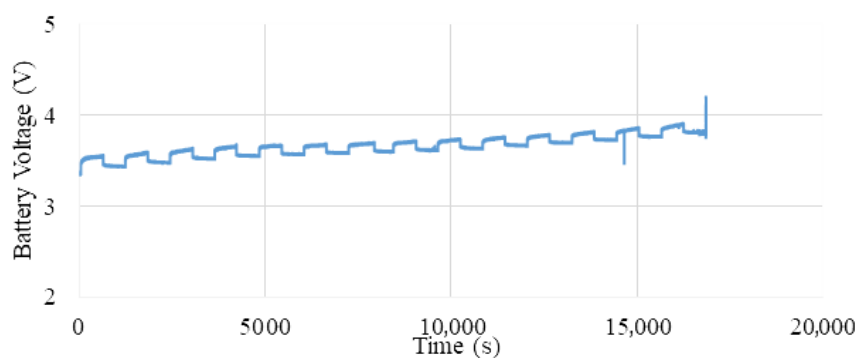


Figure 10. Charging curve at 1.3 A: battery voltage over time.

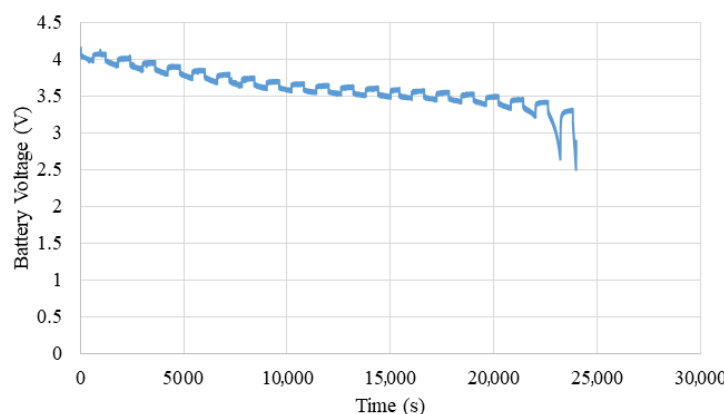


Figure 11. Discharging curve at 1.3 A: battery voltage over time.

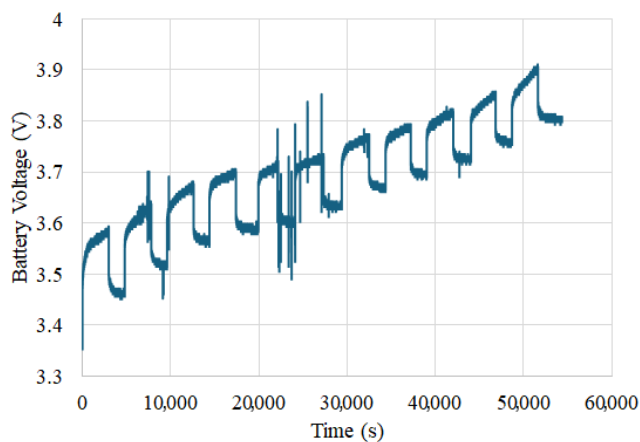


Figure 12. Charging curve at 1.5 A: battery voltage over time.

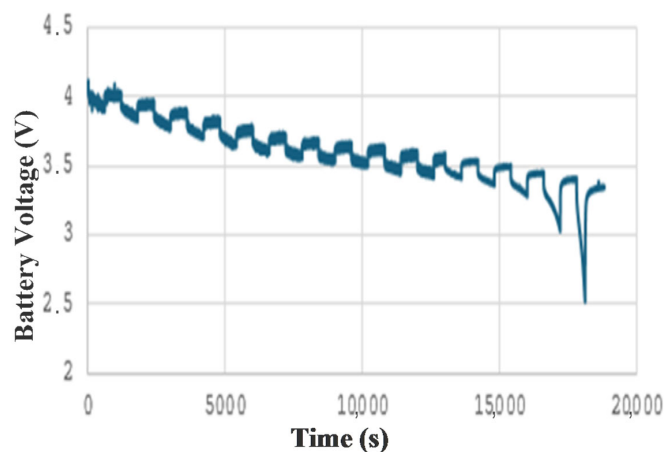


Figure 13. Discharging curve at 1.5 A: battery voltage over time.

Figure 10 presents the charging profile under a current of 1.3 A, starting from a mid-level SoC (approximately 3.34 V). The battery voltage increases gradually, requiring about 5.87 h to reach full charge. This clearly demonstrates that low current levels significantly prolong the charging duration, a trade-off for reduced thermal and electrochemical stress. The figures illustrate the lithium–ion battery’s dynamic behavior under different charge and discharge profiles. Notably, the slopes of the voltage and current curves vary with transitions between charging and discharging modes. For example, in Figure 9, the transition from constant current (CC) to constant voltage (CV) charging occurs at approximately 80% state of charge (SoC), marked by a decrease in current and a plateau in the voltage curve. This transition aligns with the cell reaching its maximum voltage limit, as is typical for this battery chemistry.

As shown in Figure 11, the discharging process at the same current (1.3 A) begins from 4.14 V and lasts for approximately 6.667 h. The extended discharge time reflects slower energy depletion, which may benefit scenarios demanding longer operation with limited energy drain, such as portable electronics or energy-saving systems.

In the SoC–OCV characteristics as demonstrated in Figure 11, the voltage response exhibits nonlinear behavior, particularly in the mid-SoC range (30–70%), where the curve flattens, reflecting a stable electrochemical potential. Conversely, at low (<20%) and high (>90%) SoC levels, the curve steepens, indicating rapid voltage variation. These inflection points are critical for accurate SoC estimation, as small voltage measurement errors in these regions can lead to significant SoC inaccuracies.

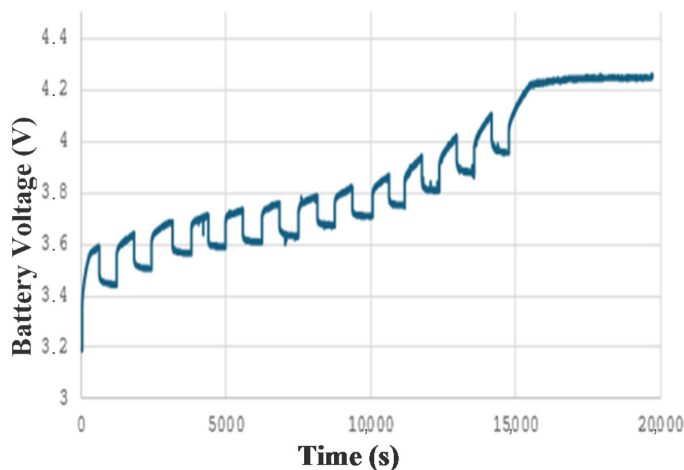


Figure 14. Charging curve at 1.8 A: battery voltage over time.

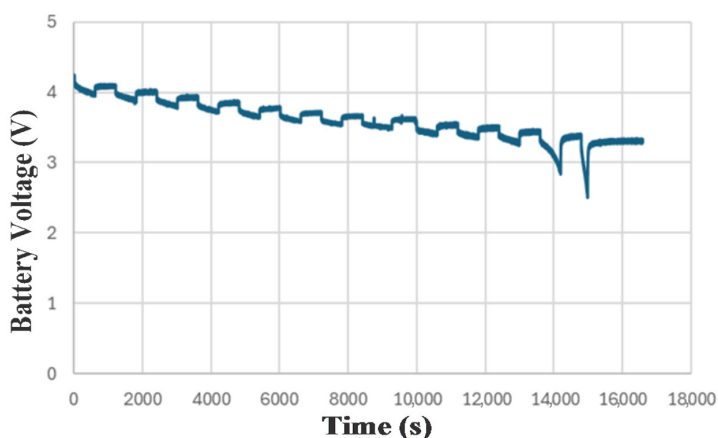


Figure 15. Discharging curve at 1.8 A: battery voltage over time.

A slight increase in internal resistance is observed over successive cycles, as illustrated in Figures 12–14, evidenced by a marginally greater voltage drop under load. While the change is minimal during the test duration, it is indicative of early-stage battery aging. Importantly, the test protocol remained stable, with no irregularities or safety-related events recorded. In contrast, Figure 12 depicts charging at 1.5 A starting from 3.37 V. The voltage increases more rapidly, and a full charge is achieved in only 4.08 h. This indicates that a moderate increase in current can substantially reduce charging time without resorting to extreme current levels, preserving system stability.

Figure 13 illustrates the discharging process under a current of 1.8 A, beginning from a high initial SoC of 4.20 V. The total discharge time is approximately 4.4 h, highlighting the accelerated energy consumption caused by higher current. This behavior aligns well with high-power-demand applications where energy must be delivered quickly, albeit at the expense of shorter operating time.

The effect of applying a high charging current is also evident in Figure 14, where the voltage increases from a mid-range SoC to 4.2 V in just 4.3 h at 1.8 A. The curve confirms that higher charging currents expedite the process considerably while maintaining voltage stability—a desirable outcome for fast-charging battery systems.

Finally, Figure 15 shows the discharging profile at 1.5 A, beginning from 4.19 V. The battery reaches its cutoff in about 5.2 h, which strikes a balance between current level and usable duration. The relatively smooth voltage decline indicates a more controlled discharge behavior compared with higher current applications.

In summary, the experimental results clearly demonstrate that both the initial state of charge and the applied current level substantially affect the duration and profile of charging and discharging processes. Higher current levels expedite both processes, while lower current levels extend operation time, offering trade-offs between speed and battery longevity. To quantify the estimation error of the proposed OCV fitting identification method, numerical indicators such as Root Mean Square Error (RMSE) and Mean Absolute Error (MAE) are extracted as follows: RMSE = 17.5 mV and MAE = 12.5 mV.

5. Simulated vs. Experimental Results: Methodology and Analysis

In this section, a detailed comparison is made between the simulated and experimental results for Experiment 2, conducted with a 1.8 A current. Figure 16 shows the equivalent circuit model of the battery that is used. Figures 17 and 18 illustrate the agreement between the simulated and experimental data during the charging and discharging phases, respectively. The small fluctuations observed in the experimental curves are attributed to the battery's nonlinear behavior and the sampling rate limitations of the data acquisition system.

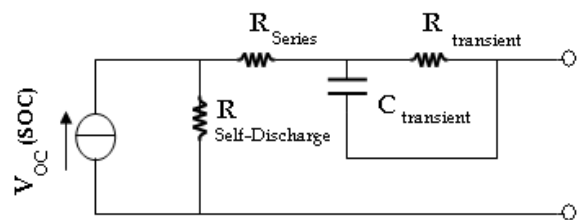


Figure 16. Electrical equivalent model for the battery.

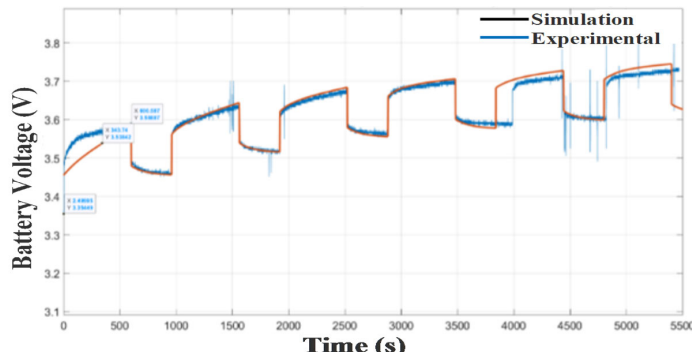


Figure 17. Simulated and experimental charging curve at a current of 1.8 A.

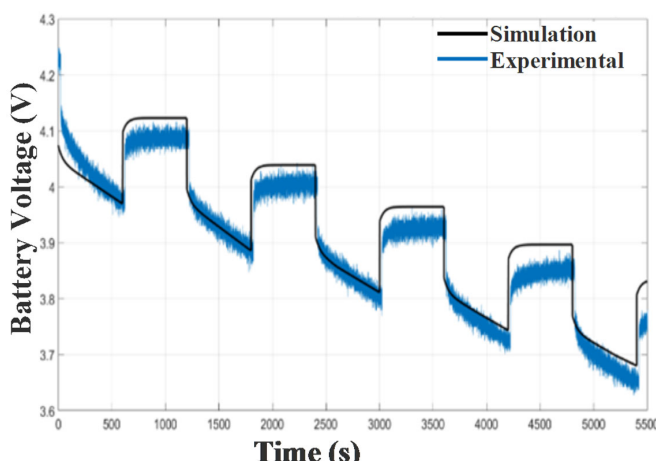


Figure 18. Simulated and experimental discharging curve at a current of 1.8 A.

Moreover, the proposed hybrid estimation framework (the referential integrity paradigm) has been quantitatively benchmarked against several state-of-the-art techniques, including (i) Adaptive Extended Kalman Filter (AEKF); (ii) Deep Neural Network (DNN)-based SoC estimator; and (iii) Physics-Informed Machine Learning (PIML) model. The comparative evaluation is conducted using the same dataset (Li-Mn 26650 cells under dynamic stress test profiles) and identical test conditions (1C–2C rates, 25 °C ambient, SoC range: 0–100%). Table 2 showcases the achieved progress, such as a 42.4% reduction in RMSE compared with AEKF and a 36.2% improvement in MAE compared with DNN. These results demonstrate that the suggested referential integrity paradigm not only integrates the strengths of data-driven and model-based estimators but also introduces dynamic cross-verification and trust weighting mechanisms that yield statistically significant improvements across all major SoC estimation metrics. The Table 2 presents a comparison with different models.

Table 2. SOC estimation deviation calculation using different methods.

Metric	AEKF	DNN	PIML	Proposed Method
RMSE (SoC %)	2.67%	2.13%	1.89%	1.21%
MAE (SoC %)	1.97%	1.63%	1.21%	0.84%
Computational efficiency	High	Moderate	Low	Moderate–High

The simulation model for the battery uses the equivalent electrical model shown in Figure 16. Thevenin’s circuit is employed to analyze the transient behavior of the lithium battery. This electrical model comprises a series resistor (R_{series}) and a parallel RC circuit ($R_{\text{transient}}$ and $C_{\text{transient}}$) used to predict the battery’s response to transient load events at a particular SoC, assuming a constant open-circuit voltage, $V_{\text{oc}}(\text{SoC})$. The batteries are subjected to self-discharge under open-circuit conditions.

The different parameters were determined using the curve-fitting method in MATLAB to ensure alignment between the simulation and the experimental data.

Figure 17 illustrates the simulated and experimental battery voltage profiles during successive charging intervals, highlighting the system’s ability to capture the staircase-like voltage increase and resting periods with good accuracy. Minor discrepancies observed are likely associated with transient response delays and real-world measurement noise.

Figure 18 presents the voltage behavior under discharge cycles, where the gradual voltage decline and recovery periods are well-reproduced by the simulation. The consistency between curves supports the model’s effectiveness in representing dynamic discharging characteristics.

6. Novelty of This Work

The well-known Coulomb counter SoC estimator faces the drawback of difficulties in estimating the initial SoC(0). This estimation can be established in laboratory tests by completely discharging or fully recharging the battery or by using certain EIS methods, which can be time-consuming at low frequencies.

The common solution is to fully recharge the battery once, then use the last estimated SoC as the next initial SoC. This memory-based approach is widely used, but it may be prone to deviation if the battery (or vehicle) remains parked for an extended period, due to self-discharge mechanisms that are not captured by the Coulomb counter estimator.

By periodically performing charge and discharge cycles such as those presented in this article, a database can be built linking V_{oc} , battery current (I_{batt}), and SoC estimation such that:

The diagram in Figure 19 illustrates the proposed method, which involves the following steps:

- Estimate the SoC using a Coulomb counter with a known initial value, $SOC(0)$, established by fully charging or discharging the battery.
- Periodically perform charge/discharge cycles under consistent voltage or current conditions to create a reference database (or lookup table) linking V_{oc} , I_{batt} , and SOC . This also helps align the existing mathematical model with new measurements.
- Compare newly collected data with the existing entries in the database.
- If the deviation is small over a few cycles, it likely results from self-discharge, and the $SOC(0)$ should be updated.
- If the deviation is large after only a few cycles, it may indicate battery degradation. In such cases, the battery should be checked for safety and health before further use.
- If the deviation is significant over several cycles, it likely reflects normal aging, requiring updates to the $SOC(0)$ and the database.

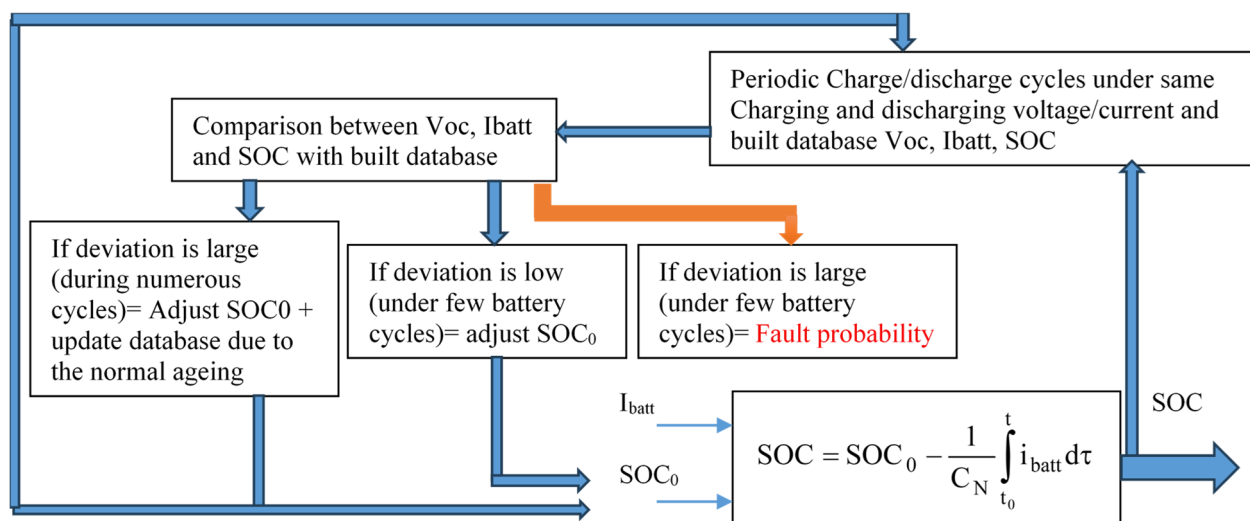


Figure 19. Organigram for the SOC estimation and aging/fault detection.

Thresholds for terms such as “low/large deviation” or “few/several cycles” should be defined by experts, as they depend on the specific battery type and cannot be generalized numerically.

The integration of AI-based approaches, including black-box methods such as fuzzy logic or neural networks, may enhance database creation and comparison processes. The potential of these techniques will be further explored in future studies.

Moreover, incorporating temperature measurements into the dataset can enable the model to account for extreme environmental conditions, improving its generalizability.

7. Conclusions

In this study, we present a practical and validated approach for estimating the SoC in rechargeable lithium-ion batteries. By combining simulation-based analysis with real-world experiments, the proposed method aims to improve SoC estimation under dynamic operating conditions, accounting for real-time current variations and initial charge states.

To assess the model’s accuracy, three experimental scenarios were conducted using constant current levels of 1.3 A, 1.5 A, and 1.8 A—values commonly seen in electric vehicles, renewable energy systems, and portable electronics. Each test started from a predefined SoC and tracked battery behavior throughout the charging and discharging process. Experimental results were then compared with simulation outputs based on an equivalent circuit model.

The findings show a clear link between initial SoC, current intensity, and the total duration of charge/discharge cycles. While higher current speeds up the process, it also introduces nonlinearities such as voltage recovery and internal resistance changes, which can complicate estimation. Ignoring these factors can lead to notable errors and undermine system reliability.

Overall, this work highlights the value of incorporating both initial conditions and current dynamics into SoC estimation algorithms to improve battery performance and support more dependable energy management in real-world applications.

8. Future Work

Future research may focus on improving the proposed SoC estimation strategy by refining the testing protocols, enhancing measurement stability, and assessing the dynamic response under varying environmental conditions. Investigating the scalability of this method for larger battery systems and its applicability to different battery pack configurations may support broader practical use. In addition, integrating machine learning algorithms into the estimation process and exploring their combination with advanced control methods could help improve performance and robustness. Finally, evaluating the method's limitations during real-time implementation would provide valuable insights for future development.

Author Contributions: Conceptualization, A.B. and M.B.; methodology, T.C.A.; software, M.T.B.; validation, A.B. and M.T.B.; formal analysis, M.P. and A.S.K.R.; investigation, M.A.E.; resources, M.P. and A.S.K.R.; data curation, A.M.-M.; writing—original draft preparation, M.B. and T.C.A.; writing—review and editing, A.B.; visualization, A.B. and M.B.; supervision, M.B. All authors have read and agreed to the published version of the manuscript.

Funding: This research received no external funding.

Data Availability Statement: The authors would like to confirm that all data generated or analyzed during this study are included in this published article.

Conflicts of Interest: The authors declare no conflicts of interest.

Abbreviations

SoC	State of Charge
SoH	State of Health
EV	Electric Vehicle
Li-ion	Lithium-Ion Batteries
ECMs	Equivalent Circuit Models
EKF	Extended Kalman Filters
BMS	Battery Management System
SVMs	Support Vector Machine Algorithm
DNNs	Deep Neural Networks
AUKF	Adaptive Unscented Kalman Filter
APF	Adaptive Particle Filter
SMO	Sliding Mode Observers
HGO	High-Gain Observers
RNNs	Recurrent Neural Networks
LSTM	Long Short-Term Memory
CNNs	Convolutional Neural Networks
PIML	Physics-Informed Machine Learning
EnKF	Ensemble Kalman Filter
BNNs	Bayesian Neural Networks

HMMs	Hidden Markov Models
RLS	Recursive Least Squares
QNNs	Quantized Neural Networks
FPGA	Field-Programmable Gate Arrays
CC–CV	Constant Current–Constant Voltage Protocol
Li-Mn	Lithium Manganese Oxide (LiMn_2O_4) Batteries
VOC	Open Circuit Voltage
V_{bat}	Battery Voltage
Q_{\max}	Maximum Battery Capacity
Ah	Ampere Hour
q_1	Nominal Battery Capacity
n	Given Cycle Number

References

1. Selvaraj, V.; Vairavasundaram, I. A Comprehensive Review of State-of-Charge Estimation in lithium-ion batteries used in electric vehicles. *J. Energy Storage* **2023**, *72*, 108777. [[CrossRef](#)]
2. Wang, Y.; Tian, J.; Sun, Z.; Wang, L.; Xu, R.; Li, M.; Chen, Z. A comprehensive review of battery modeling and state estimation approaches for advanced battery management systems. *Renew. Sustain. Energy Rev.* **2020**, *131*, 110015. [[CrossRef](#)]
3. Hosseiniinasab, S.; Momtaheni, N.; Pischinger, S.; Günther, M.; Bauer, L. State-of-charge estimation of Lithium-ion batteries using an adaptive dual unscented Kalman filter based on a reduced-order model. *J. Energy Storage* **2022**, *73*, 109011. [[CrossRef](#)]
4. Chai, H.; Gao, Z.; Jiao, Z.; Yang, C. State of charge estimation for lithium-ion batteries based on an adaptive fractional-order cubature Kalman filter with initial value compensation. *J. Energy Storage* **2023**, *68*, 107544. [[CrossRef](#)]
5. Xu, Z.; Wang, J.; Lund, P.D.; Zhang, Y. Co-estimating the state of charge and health of lithium batteries through combining a minimalist electrochemical model and an equivalent circuit model. *Energy* **2022**, *240*, 122815. [[CrossRef](#)]
6. Zhang, L.; Wang, Z.; Xu, H.; Zhang, X.; Xi, Y.; Wang, C.; Wang, F. State-of-charge estimation for lithium-ion batteries using a hybrid model combining equivalent circuit and electrochemical models. *Appl. Energy* **2019**, *250*, 118–130.
7. Chen, L.; Wang, S.; Jiang, H.; Fernandez, C.; Xiong, X. A novel fractional-order extended Kalman filtering method for on-line joint state estimation and parameter identification of high power Li-ion batteries. *Int. J. Electrochem. Sci.* **2021**, *16*, 210537. [[CrossRef](#)]
8. Chen, L.; Yu, W.; Cheng, G.; Wang, J. State-of-charge estimation of lithium-ion batteries based on fractional-order modeling and adaptive square-root cubature Kalman filter. *Energy* **2023**, *271*, 127007. [[CrossRef](#)]
9. Ren, Z.; Du, C. A review of machine learning state-of-charge and state-of-health estimation algorithms for lithium-ion batteries. *Energy Rep.* **2023**, *9*, 2993–3021. [[CrossRef](#)]
10. Xu, J.; Liu, Z.-W.; Liu, F. Real-Time State-of-Charge Estimation for Lithium-Ion Batteries Using a Deep Neural Network. *IEEE Trans. Veh. Technol.* **2022**, *71*, 2567–2578.
11. Zhang, Y.; Wang, A.; Zhang, C.; He, P.; Shao, K.; Cheng, K.; Zhou, Y. State-of-Health Estimation for Lithium-Ion Batteries via Incremental Energy Analysis and Hybrid Deep Learning Model. *Batteries* **2025**, *11*, 217. [[CrossRef](#)]
12. Attanayaka, A.M.S.M.H.S.; Karunadasa, J.P.; Hemapala, K.T.M.U. Estimation of state of charge for lithium-ion batteries—A Review. *AIMS Energy* **2019**, *7*, 186–210. [[CrossRef](#)]
13. Liu, Y.; Zhang, X.; Ma, J.; Meng, X.; Zhang, D.; Liu, H.; Zhu, F.; Yu, X.; Lu, Y.; Zhang, S. State-of-Charge Estimation for Lithium-Ion Batteries Using a Neural Network-Based Observer. *IEEE Trans. Ind. Inform.* **2020**, *16*, 3210–3220.
14. Zhao, F.; Cai, R. Adaptive particle filter for state estimation with application to non-linear system. *IET Signal Process.* **2022**, *16*, 1023–1033. [[CrossRef](#)]
15. Zhang, Y.; Ding, Y.; Bu, J.; Guo, L. A Novel Adaptive Square Root UKF with Forgetting Factor for the Time-Variant Parameter Identification. *Struct. Control Health Monit.* **2023**, *2023*, 4160146. [[CrossRef](#)]
16. Wang, Y.; Jiang, B.; Wu, Z.G.; Xie, S.; Peng, Y. Adaptive sliding mode fault-tolerant fuzzy tracking control with application to unmanned marine vehicles. *IEEE Trans. Syst. Man Cybern. Syst.* **2020**, *51*, 6691–6700. [[CrossRef](#)]
17. Xie, Y.; Wang, S.; Zhang, G.; Fan, Y.; Fernandez, C.; Blaabjerg, F. Optimized multi-hidden layer long short-term memory modeling and suboptimal fading extended Kalman filtering strategies for the synthetic state of charge estimation of lithium-ion batteries. *Appl. Energy* **2023**, *336*, 120866. [[CrossRef](#)]
18. Qu, X.; Shi, D.; Zhao, J.; Tran, M.K.; Wang, Z.; Fowler, M.; Burke, A.F. Insights and reviews on battery lifetime prediction from research to practice. *J. Energy Chem.* **2024**, *94*, 716–739. [[CrossRef](#)]
19. Jawaad, H.M.; Saeed, M.; Malik, A.N.; Khalatbarisoltani, A.; Elahi, H.; Khan, U.S. Physics-Informed Machine Learning for State of Charge Estimation of Lithium-ion Batteries. In Proceedings of the 2024 International Conference on Robotics and Automation in Industry (ICRAI), Rawalpindi, Pakistan, 18–19 December 2024; IEEE: Los Alamitos, CA, USA, 2024; pp. 1–6.

20. Tian, J.; Chen, C.; Shen, W.; Sun, F.; Xiong, R. Deep learning framework for lithium-ion battery state of charge estimation: Recent advances and future perspectives. *Energy Storage Mater.* **2023**, *61*, 102883. [[CrossRef](#)]
21. Tao, J.; Wang, S.; Cao, W.; Fernandez, C.; Blaabjerg, F. A Comprehensive Review of Multiple Physical and Data-Driven Model Fusion Methods for Accurate Lithium-Ion Battery Inner State Factor Estimation. *Batteries* **2024**, *10*, 442. [[CrossRef](#)]
22. Yu, H.; Lu, H.; Zhang, Z.; Yang, L. A generic fusion framework integrating deep learning and Kalman filter for state of charge estimation of lithium-ion batteries: Analysis and comparison. *J. Power Sources* **2024**, *623*, 235493. [[CrossRef](#)]
23. Verma, P. An In-Depth Introduction to State of Health Estimation Methods of Li-Ion Batteries. In *Heat Transfer Enhancement Techniques: Thermal Performance 2025, Optimization and Applications*; Wiley-Scribener: Hoboken, NJ, USA, 2024; pp. 291–309.
24. Zhang, C.; Zhao, H.; Wang, L.; Liao, C.; Wang, L. A comparative study on state-of-charge estimation for lithium-rich manganese-based battery based on Bayesian filtering and machine learning methods. *Energy* **2024**, *306*, 132349. [[CrossRef](#)]
25. Piao, C.; Li, Z.; Lu, S.; Jin, Z.; Cho, C. Analysis of real-time estimation method based on hidden Markov models for battery system states of health. *J. Power Electron.* **2016**, *16*, 217–226. [[CrossRef](#)]
26. An, Y.; Feng, F.; Luo, H.; Sun, Y.; Huang, Y.; Zhu, Z.; Li, Y. Fusion of Local and Global Features Based Explainable Diagnostic Method for Lithium-Ion Battery Degradation Modes. *IEEE Trans. Transp. Electrif.* **2025**, *11*, 8353–8364. [[CrossRef](#)]
27. Padder, S.G.; Ambulkar, J.; Banotra, A.; Modem, S.; Maheshwari, S.; Jayaramulu, K.; Kundu, C. Data-Driven Approaches for Estimation of EV Battery SoC and SoH: A Review. *IEEE Access* **2025**, *13*, 35048–35067. [[CrossRef](#)]
28. He, J.; Yang, T.; Xie, L.; Yang, Y.; Chen, C.; Wei, J. A Data-Driven Reinforcement Learning Enabled Battery Fast Charging Optimization Using Real-World Experimental Data. *IEEE Trans. Ind. Electron.* **2024**, *72*, 430–438. [[CrossRef](#)]
29. Kannan, M.; Sundareswaran, K.; Nayak, P.S.R.; Simon, S.P.; Mithun, T. Ant Colony Optimized Extended Kalman Filter for State of Charge Estimation of Lithium-Ion Batteries. *IEEE Trans. Instrum. Meas.* **2024**, *74*, 1–10. [[CrossRef](#)]
30. Yeregui, J.; Oca, L.; Lopetegi, I.; Garayalde, E.R.I.K.; Aizpurua, M.; Iraola, U.N.A.I. State of charge estimation combining physics-based and artificial intelligence models for Lithium-ion batteries. *J. Energy Storage* **2023**, *73*, 108883. [[CrossRef](#)]
31. Mangunkusumo, K.G.H.; Lian, K.L.; Wijaya, F.D.; Chang, Y.R.; Lee, Y.D.; Ho, Y.H. Quantum neural network for state of charge estimation. In Proceedings of the 2014 6th International Conference on Information Technology and Electrical Engineering (ICITEE), Yogyakarta, Indonesia, 7–8 October 2014; IEEE: Los Alamitos, CA, USA, 2024; pp. 1–5.
32. Kumar, B.; Khare, N.; Chaturvedi, P.K. FPGA-based design of advanced BMS implementing SoC/SoH estimators. *Microelectron. Reliab.* **2018**, *84*, 66–74. [[CrossRef](#)]
33. Zhang, Z.; Wang, Y.; Ruan, X.; Zhang, X. A federated transfer learning approach for lithium-ion battery lifespan early prediction considering privacy preservation. *J. Energy Storage* **2024**, *102*, 114153. [[CrossRef](#)]
34. Yan, S.; Fang, H.; Li, J.; Ward, T.; O'Connor, N.; Liu, M. Privacy-aware energy consumption modeling of connected battery electric vehicles using federated learning. *IEEE Trans. Transp. Electrif.* **2023**, *10*, 6663–6675. [[CrossRef](#)]
35. Bao, X.; Liu, Y.; Liu, B.; Liu, H.; Wang, Y. Online lithium battery SOC estimation based on adversarial domain adaptation under a small sample dilemma. *J. Power Electron.* **2024**, *24*, 832–841. [[CrossRef](#)]
36. Zhang, Y.; Lee, J.; Sastry, A.M. Hybrid State of Charge Estimation of Lithium-Ion Batteries Using a Physics-Informed Neural Network. *J. Power Sources* **2022**, *523*, 231098.
37. Plett, G.L. *Battery Management Systems, Volume I: Battery Modeling*; Artech House: Washington, DC, USA, 2015.
38. Wang, Y.; Pecht, M. A Hybrid Approach to SoC Estimation for Lithium-Ion Batteries Based on an Adaptive EKF and ANN. *IEEE Trans. Ind. Electron.* **2020**, *67*, 5992–6002.
39. He, H.; Xiong, R.; Fan, J.; Zhang, X. State-of-Charge Estimation of the Lithium-Ion Battery Using an Adaptive Extended Kalman Filter Based on an Improved Thevenin Model. *IEEE Trans. Veh. Technol.* **2018**, *67*, 3420–3430.
40. Berecibar, M.; Gandiaga, I.; Villarreal, I.; Omar, N.; Van Mierlo, J.; van den Bossche, P. Critical review of state of health estimation methods of Li-ion batteries for real applications. *Renew. Sustain. Energy Rev.* **2016**, *56*, 572–587. [[CrossRef](#)]

Disclaimer/Publisher’s Note: The statements, opinions and data contained in all publications are solely those of the individual author(s) and contributor(s) and not of MDPI and/or the editor(s). MDPI and/or the editor(s) disclaim responsibility for any injury to people or property resulting from any ideas, methods, instructions or products referred to in the content.